Journal of the European Ceramic Society xxx (xxxx) xxx–xxx

Contents lists available at ScienceDirect

Journal of the European Ceramic Society

journal homepage: www.elsevier.com/locate/jeurceramsoc

Original Article

Impact of additives and processing on microstructure and dielectric properties of willemite ceramics for LTCC terahertz applications

B. Synkiewicz-Musialska[a], D. Szwagierczak[a,*], J. Kulawik[a], N. Pałka[b], P.R. Bajurko[c]

[a] Research Network Łukasiewicz, Institute of Electron Technology, Kraków Division, Kraków, Poland
[b] Military University of Technology, Institute of Optoelectronics, Warszawa, Poland
[c] Warsaw University of Technology, Institute of Radioelectronics and Multimedia Technology, Warszawa, Poland

ARTICLE INFO

Keywords:
Willemite Zn_2SiO_4
LTCC
Microwave ceramics
Dielectric properties
THz time domain spectroscopy

ABSTRACT

The paper presents the fabrication procedure, microstructure and dielectric properties of the low temperature cofired ceramics (LTCC) based on Zn_2SiO_4 doped with AlF_3, CaB_4O_7, Li_2TiO_3 and $MgTiO_3$. The heating microscope studies and differential thermal analysis were used for characterization of the behavior of the green tapes and ceramic samples during heating up to high temperatures. The microstructure and composition were analyzed by scanning electron microscopy, X-ray energy dispersive spectroscopy and XRD method. The dielectric properties were investigated in three frequency regions: 100 Hz–2 MHz, 90–140 GHz and 0.15–3 THz. The developed materials are promising candidates for the LTCC submillimeter wave applications due to a low sintering temperature of 900–980 °C, good compatibility with silver pastes and good dielectric properties – a low dielectric permittivity of 6–6.8, a relatively low dissipation factor of 0.005–0.008 at 1 THz, and a weak temperature dependence of dielectric permittivity.

1. Introduction

Permanent progress in mobile telecommunication, wireless local area networks, antennas, radar systems, etc. requires expanding of the operating frequency of devices up to the terahertz range. A higher signal propagation speed, lower attenuation, narrower tuning, better temperature stability are the priority goals for new microwave substrate materials. The materials with low dielectric permittivity, low dielectric loss and close to zero temperature coefficient of resonant frequency meet these requirements [1–3]. The ceramic materials exhibiting low dielectric permittivity comprise quartz, cristobalite, cordierite, forsterite, diopside, zinc borates, borosilicate glasses, glass-ceramics with a high SiO_2 or B_2O_3 content [4–8]. Among these materials, willemite Zn_2SiO_4 is one of the best candidates [9–20].

Willemite crystallizes in the trigonal system, spatial group R-3. It is an orthosilicate built of the tetrahedra containing zinc and silicon in three different crystallographic positions [9]. These are two slightly different positions of Zn I (Zn-O - 1.950 Å) and Zn II (Zn-O - 1.961 Å) and Si (Si-O- 1.635 Å). Crystallization of β-Zn_2SiO_4 and α-Zn_2SiO_4 takes place at 750 °C and 950 °C, respectively. The Zn-O bonds exhibit high covalence due to the strong hybridization of Zn3d orbitals with O2p orbital (sp3 hybridization) which promotes the particularly short Zn-O distances [9].

Willemite shows good mechanical properties, high thermal conductivity, low thermal expansion coefficient and very interesting optical properties, which are related to the rigid network with the non-centrosymmetric cation positions [10]. Synthetic willemite (doped with Mn^{2+}, Tb^{3+}, Ce^{3+}, Eu^{3+}) is widely used as a luminescent material (kinescopes, fluorescent lamps, plasma displays) due to the saturated color (green, yellow, red), strong luminescence and high chemical and thermal stability. The manganese-doped Zn_2SiO_4 is used in medical imaging, especially in mammography. The cobalt-doped willemite is a potential candidate for the use in the visible and near-infrared lasers. It is also used as a blue ceramic pigment with high temperature stability [10]. However, reports about the implementation of willemite ceramics for the LTCC microwave substrates are very scarce.

Eidem et al. [11] studied the phase equilibria in the ZnO-SiO_2 system. At temperatures above 800 °C, the only stable phase in this system is zinc orthosilicate α-2ZnO·SiO_2. Guo et al. [12] reported willemite ceramics Zn_2SiO_4 with the excellent millimeter-wave dielectric properties: a dielectric permittivity of 6.6, a quality factor (Qxf) of 219,000 GHz and a temperature coefficient of resonant frequency (τ_f) of −61 ppm/°C. To attain the desired, near zero τ_f value and to lower the sintering temperature, the addition of TiO_2 was used. The optimal properties were achieved for the ceramics with 11 wt.% TiO_2, sintered at 1250 °C: ε_r = 9.3, Qxf = 113,000 GHz and τ_f = 1 ppm/°C.

* Corresponding author.
E-mail address: dszwagi@ite.waw.pl (D. Szwagierczak).

https://doi.org/10.1016/j.jeurceramsoc.2019.10.005
Received 11 July 2019; Received in revised form 2 October 2019; Accepted 3 October 2019

LTCC is an emerging technology for microwave packaging due to its potential for miniaturization, embedding passive components and multifunctionality. A significant progress concerns both the commercial green tapes and the new research results. The A6M LTCC tape offered by the Ferro company shows a low and stable dielectric constant of about 6 and a very low loss tangent below 0.002 over a wide, high frequency range of 1–100 GHz [21]. In the last decade, among the intensively explored materials for microwave substrates, have been those with the ultra-low sintering temperature (ULTCC) that are based mainly on the systems rich in Li_2O, MoO_3, WO_3, TeO_2, Bi_2O_3 and V_2O_5 and compatible with the cheap Ag or Al thick film conductive pastes [22–24]. Recently, "cold sintering" at temperatures below 200 °C has been used as a promising method for the preparation of microwave ceramics and composites [25,26].

For the willemite based ceramics, lowering of its high sintering temperature (about 1300 °C) is necessary to make it suitable for LTCC technology. Literature devoted to this topic is confined to a few papers. A low sintering temperature of 950 °C, adjusted to the LTCC technology, was reported for the Zn_2SiO_4-$Zn_3B_2O_6$ composite that exhibited good microwave dielectric properties: $\varepsilon_r = 6.1$ and quality factor of 94 300 GHz [13]. A nonstoichiometric material of the nominal composition $Zn_{1.8}SiO_{3.8}$ with the addition of 20 mol % of B_2O_3 was sintered at 900 °C and showed very good microwave properties: $\varepsilon_r = 5.7$, $Qxf = 53{,}000$ GHz and $\tau_f = -16$ ppm/°C [14]. During firing of this material, B_2O_3 reacted with the remnant SiO_2 to form a liquid phase which contributed to the densification process. The addition of 4 wt.% Li_2CO_3-H_3BO_3 to $0.95Zn_2SiO_4$-$0.05CaTiO_3$ composite resulted in decreasing of the sintering temperature to 950 °C [15]. This material was characterized by a low dielectric permittivity of 7.1, $Qxf = 26\,300$ GHz, a near zero τ_f of -4.5 ppm/°C and good chemical compatibility with silver.

The present research was aimed at the fabrication and characterization of the green tapes as well as testing of the multilayer LTCC structures based on willemite ceramics with the sintering temperatures which were lowered, using AlF_3-CaB_4O_7, Li_2TiO_3 and $MgTiO_3$. Time domain spectroscopy was used to investigate dielectric properties of the developed ceramics at the very high frequencies in the THz range. To the best of our knowledge, such measurements have not yet been performed for these materials. Search for the new materials for advanced substrates and packages is justified by a wide and not fully recognized potential application scope of the THz radiation. Progress in miniaturization, signal speed and integration scale of telecommunication systems is the obvious profit of using the THz spectral region. Furthermore, the nonionizing nature of this radiation, which is safe for humans and nondestructive for electronic circuits as well as imaging possibilities in infrared blind conditions (e.g. dust, smoke, fog, rain) create new perspectives in the medical, biochemical, and security areas.

2. Experimental

A conventional solid state reaction method was used for the synthesis of Zn_2SiO_4. Reagent grade powders of ZnO and SiO_2 were weighed in the stoichiometric proportions, milled in isopropyl alcohol using a Fritsch ball mill and agate grinding media, pelletized and calcined at 1150 °C for 8 h. Then the reaction product was crushed and ball milled for 8 h. The XRD analysis confirmed a single phase composition of the synthesized willemite.

Three additives were used for diminishing the sintering temperature of pure willemite ceramics: a mixture of AlF_3 and CaB_4O_7 (in 1:1 M ratio), a mixture of AlF_3, CaB_4O_7 and Li_2TiO_3 (in 1:1:3 M ratio) and a mixture of AlF_3-CaB_4O_7 with $MgTiO_3$ (in 1:1 wt ratio). The batches containing the willemite powder and 2–10 wt.% of the additives were prepared by mixing the components in the planned proportions and ball milling for 8 h.

An optimal level of the additives ensuring adequate lowering of the sintering temperature was established using a Leitz heating microscope. The obtained ceramic powders were utilized for preparation of the bulk ceramic samples and green tapes. For the bulk ceramics, the powders were granulated with polyvinyl alcohol, pressed into discs using a uniaxial press and sintered at 900–980 °C for 1–8 h. For green tapes preparation, the ceramic powders were milled with organic additives: polyvinyl butyral as a binder, fish oil as a dispersant, polyethylene glycol 400 and dibutyl phthalate as plasticizers, toluene and isopropyl alcohol as solvents. A tape caster (TTC-1200, Mistler) was used for obtainment of green tapes. The green tapes were dried at room temperature and at 50 °C for a few hours and cut by a laser (E-355-3-G-OA, Oxford Lasers) into the sheets with the planned dimensions.

The differential thermal analysis (DTA) and thermogravimetric (TG) studies of the green tapes were carried out (Netzsch STA 449 F3 thermal analyzer) in order to track the thermal effects and mass changes during heating in a temperature range of 20–1000 °C and to adjust the optimal firing profiles.

Three commercial pastes based on Ag, AgPd and Pt were used for screen printing of the test conducting patterns onto the green dielectric sheets. 10–20 green sheets were stacked and isostatically pressed under the pressure of 30 MPa at 70 °C using the IL-4008PC Pacific Trinetics Corporation laminator. The green laminates were fired according to the carefully adjusted profile with the maximum temperature of 880–980 °C held for 1–4 h.

The phase compositions of the ceramic powders sintered at optimal temperatures were determined by means of a PANalytical, model Empyrean diffractometer, using Cu $K_{\alpha 1}$ radiation. The microstructure and elemental composition of the obtained substrates as well as their cooperation with the commercial conductive pastes were investigated using a FEI scanning electron microscope (SEM) and the EDAX Genesis EDS system.

The dielectric properties of the fabricated substrates were characterized by the impedance spectroscopy method in the temperature range from −30 to 150 °C at frequencies ranging from 100 Hz to 2 MHz (Quadtech LCR meter).

The measurements in the 90–140 GHz frequency band were conducted using the set-up presented in Fig. 1. The sample was placed in the holder in such a way that it covers the circular aperture made in the sheet of the absorber. The aperture was illuminated from one side by the waves coming from the horn antenna and reflected from the off-axis parabolic mirror. On the other side there was the second parabolic mirror reflecting the waves passing through the aperture and through the sample to the second antenna. The complex transmission coefficient between two antenna ports was measured by means of the set of the vector network analyzer (VNA) and two frequency extender modules (VNAX) operating in the 90–140 GHz band.

The measurement data were processed according to the method presented previously [27] in order to determine the dielectric parameters of the sample. The accuracy of the sample thickness value has the greatest impact on the accuracy of the calculated dielectric permittivity. Therefore, the tested samples were polished to obtain a thickness tolerance of the order of 10 µm. The range of the thickness variability was measured for each particular sample and used to determine the permittivity uncertainty range. In contrast, the dissipation factor values were estimated roughly due to a contribution of the systematic errors introduced to this parameter by propagation phenomena

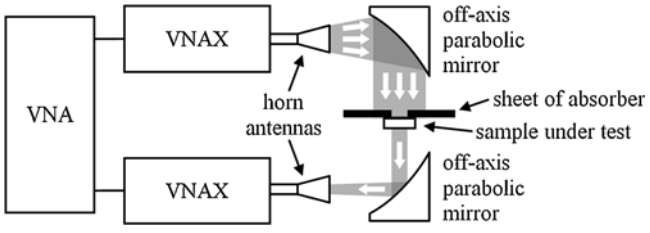

Fig. 1. Set-up for measurements in the 90–140 GHz frequency band.

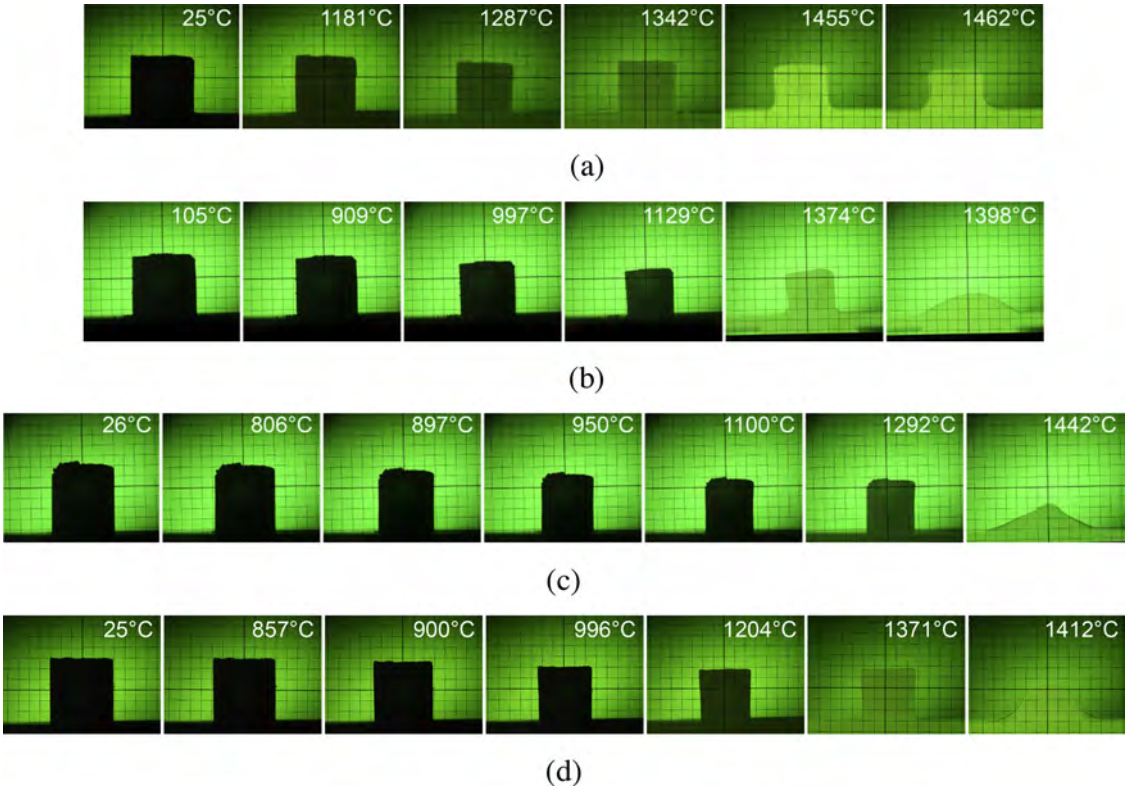

Fig. 2. Selected images from the heating microscope for: (a) willemite, (b) Zn_2SiO_4 with 5% AlF_3-CaB_4O_7, (c) Zn_2SiO_4 with 4% AlF_3-CaB_4O_7-Li_2TiO_3, (d) Zn_2SiO_4 with 5% AlF_3-CaB_4O_7 + 5% $MgTiO_3$.

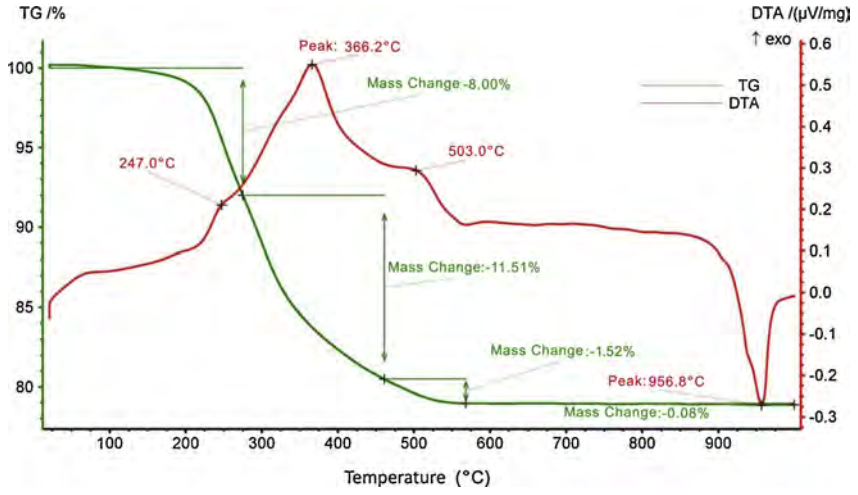

Fig. 3. Results of thermal analysis (TG and DTA curves) for Zn_2SiO_4 - 4% AlF_3-CaB_4O_7-Li_2TiO_3 green tape. (For interpretation of the references to colour in this figure legend, the reader is referred to the web version of this article).

in the absorber aperture. They result in the uneven phase distribution of the wave incident on the sample surface. This have a significant and different for each sample impact on the calculated dissipation factor, but a minor impact on the dielectric permittivity.

The dielectric measurements at the highest studied terahertz frequencies were carried out by the time domain spectroscopy. The applied setup (TeraView), which comprises an advanced optoelectronic system with a femtosecond laser, photoconductive antennas and a delay line, enabled the generation and accurate detection of a 0.5 ps electromagnetic pulse with the spectrum in the range of about 0.1–3.5 THz. The ceramic samples with the thickness of a few millimeters were placed in the holders and situated in the focal point of the terahertz beam. Purged air was used to avoid the influence of moisture from the atmosphere. Coherent detection in a transmission configuration was the source of both the transmissive and the dispersive information (the complex refractive index) about the investigated samples with a 10 GHz resolution. The measurements in the THz range were performed at room temperature. For the pure willemite ceramics, the influence of temperature changing in the 30–150 °C range was additionally studied.

3. Results and discussion

3.1. Heating microscope data and thermal analysis

The additives used as the sintering aids for willemite ceramics were chosen taking into account a low melting temperature of the additive

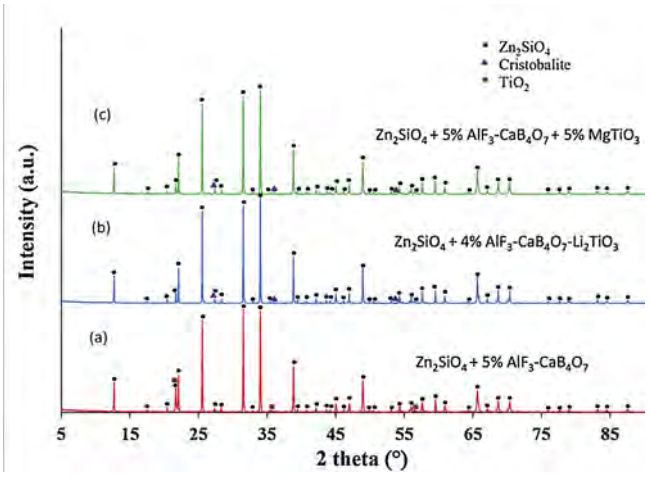

Fig. 4. XRD patterns for: (a) Zn_2SiO_4 with 5% AlF_3-CaB_4O_7, sintered at 980 °C, (b) Zn_2SiO_4 with 4% AlF_3-CaB_4O_7-Li_2TiO_3, sintered at 900 °C, (c) Zn_2SiO_4 with 5% AlF_3-CaB_4O_7 + 5% $MgTiO_3$, sintered at 930 °C.

and/or a low sintering temperature of the willemite ceramic with the additive, a relatively low dielectric permittivity of the additive, and its positive temperature coefficient of resonant frequency. The applied additives met these requirements. The analysis performed using a heating microscope (not shown) revealed that the mixtures of AlF_3 and CaB_4O_7 in 1:1 M ratio and AlF_3, CaB_4O_7 and Li_2TiO_3 in 1:1:3 M ratio form the eutectics with the relatively low melting points. The dielectric permittivities of CaB_4O_7, $MgTiO_3$ and Li_2TiO_3 are higher than that of willemite, although relatively low (11, 17 and 22, respectively) [28–31]. The main aim of the introduction of Li_2TiO_3 and $MgTiO_3$ titanates as the additives, was lowering of the temperature dependence of the dielectric permittivity since these titanates as the single phase materials exhibit the positive temperature coefficients of resonant frequency, which enable a partial compensation of the negative value of this coefficient occurring for the most low dielectric permittivity materials, including willemite. Furthermore, it was observed that Li_2TiO_3 and $MgTiO_3$ can form the low melting eutectics with the other applied additives (e.g. AlF_3-CaB_4O_7) and/or with the main Zn_2SiO_4 phase, and consequently they can act as the sintering aids decreasing the sintering temperature.

In Fig. 2 the images from the heating microscope illustrating changes in the dimensions and shape of the samples in the temperature range 20–1460 °C are compared for the pure and doped willemite. The results of heating microscope studies indicate that the applied three additives significantly decrease the sintering temperature of the pure willemite ceramics. The shrinkage of the samples starts at 1181, 909, 806 and 857 °C for pure Zn_2SiO_4, Zn_2SiO_4 doped with 5% AlF_3-CaB_4O_7, 4% AlF_3-CaB_4O_7-Li_2TiO_3 and 5% AlF_3-CaB_4O_7 + 5% $MgTiO_3$, respectively. The onset of shrinking for the doped ceramics was found to be approximately consistent with the softening temperature of the relevant additive.

The mixture with the molar composition $0.2AlF_3$-$0.2CaB_4O_7$-$0.6Li_2TiO_3$ (denominated as AlF_3-CaB_4O_7-Li_2TiO_3) has the very good properties as a sintering aid, despite its relatively high melting point of about 1200 °C. The shrinkage of this mixture starts at a low temperature of about 700 °C and softening occurs at about 930 °C. The minimum level of AlF_3-CaB_4O_7-Li_2TiO_3 additive that allows for a significant shrinkage of the willemite ceramics at a temperature of about 900 °C, advantageous for cofiring with the cheap silver electrodes, was established at 4 wt.%.

The dielectric tapes based on Zn_2SiO_4 obtained as a result of the tape casting process were smooth and flexible and showed a good mechanical strength. The thicknesses of the dried tapes were about 80 μm. The mass and temperature changes of a green Zn_2SiO_4-based dielectric tape in the temperature range 20–1000 °C are exemplified in Fig. 3 which presents the results of TG-DTA thermal analysis for the Zn_2SiO_4-4% AlF_3-CaB_4O_7-Li_2TiO_3 sample. A few broad exothermic peaks observed in the DTA curve in the temperature range 200–550 °C are related to the burnout of the binder and plasticizers from the green tape. The corresponding significant mass loss (about 13%) is evident in the TG curve. The effects for the particular organic components are partially overlapping. However, the inflection point at 247 °C and the local maxima at 366 °C and 503 °C can be attributed to the oxidation of polyethylene glycol [32], dibuthyl phthalate and polyvinyl butyral [33,34], respectively. In the range of 600–870 °C, the values of DTA and TG plots remain constant. At a temperature of 956 °C, the endothermic peak in the DTA curve is observed. It corresponds roughly to the softening temperature of the Zn_2SiO_4 sample with this additive, determined using the heating microscope and it is about 20° higher than the softening temperature of the additive alone.

3.2. XRD analysis

Fig. 4 presents the results of the XRD phase analysis of the doped willemite samples. As can be seen from Fig. 4a for the Zn_2SiO_4 powder with 5% AlF_3-CaB_4O_7, sintered at 980 °C, the dominant crystalline phase is willemite. As a minor crystalline phase, there occurs cristobalite SiO_2 (7.9%).

Figs. 4b and c illustrate the diffractograms of the Zn_2SiO_4 powder

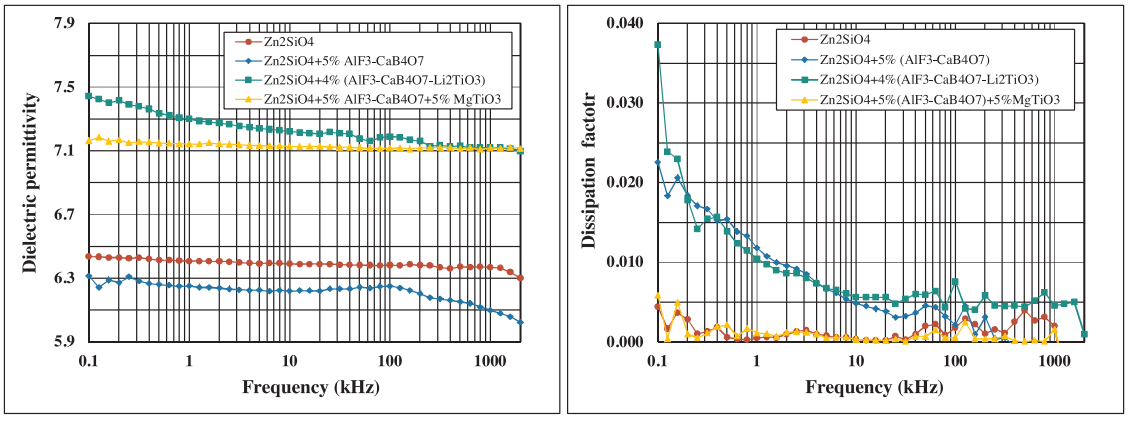

Fig. 5. Comparison of the frequency dependencies of dielectric permittivity (a) and dissipation factor (b) at 20 °C in the 100 Hz-2 MHz range for pure and doped Zn_2SiO_4 ceramics.

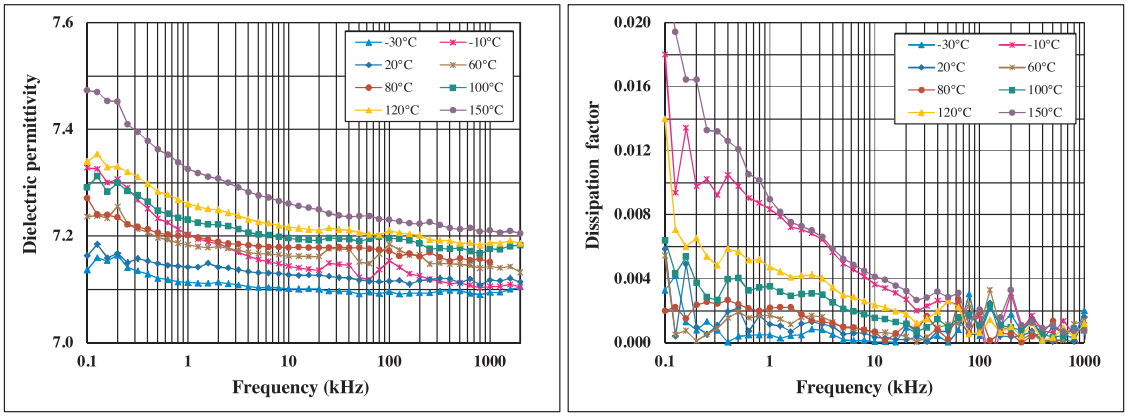

Fig. 6. Dielectric permittivity (a) and dissipation factor (b) in the temperature range from -30 to 150 °C as a function of frequency in the 100 Hz–2 MHz range for Zn_2SiO_4 with 5% AlF_3-CaB_4O_7 + 5% $MgTiO_3$, sintered at 930 °C.

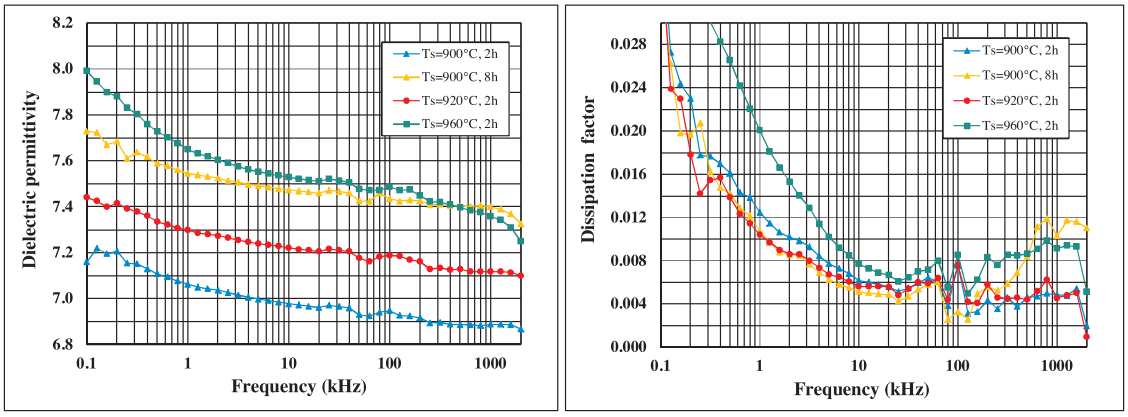

Fig. 7. Comparison of the frequency dependencies of dielectric permittivity (a) and dissipation factor (b) at 20 °C in the 100 Hz–2 MHz range for Zn_2SiO_4 with 4% AlF_3-CaB_4O_7-Li_2TiO_3, sintered in different conditions.

Table 1
Composition, sintering temperatures and dielectric properties of Zn_2SiO_4 based substrate materials.

Composition	Sintering temperature,°C	Dielectric permittivity				Dissipation factor			
		1 MHz		Mean value in the 90–140 GHz band	1 THz	1 MHz		Mean value in the 90–140 GHz band	1 THz
		20 °C	150 °C	20 °C	20 °C	20 °C	150 °C	20 °C	20 °C
Zn_2SiO_4	1320	6.4	6.5	6.1	6.0 (20 °C) 6.3 (150 °C)	0.001	0.002	≤0.005	0.005 (20 °C) 0.006 (150 °C)
Zn_2SiO_4 + 5% AlF_3-CaB_4O_7	980	6.1	6.2	6.0	6.1	0.003	0.002	≤0.005	0.008
Zn_2SiO_4- + 5% AlF_3-CaB_4O_7 + 5% $MgTiO_3$	930	7.1	7.3	6.7	6.7	0.001	0.002	≤0.007	0.009
Zn_2SiO_4- + 4% (0.2AlF_3-0.2CaB_4O_7-0.6Li_2TiO_3)	900	7.0	7.2	–	6.8	0.005	0.033	–	0.009

with 4% AlF_3-CaB_4O_7-Li_2TiO_3 and 5% AlF_3-CaB_4O_7 + 5% $MgTiO_3$, respectively. For both the samples, willemite is the main crystalline phase. Small amounts of rutile TiO_2 (1.6 and less than 3%, respectively) were also detected. The introduced additives did not appear among the revealed crystalline phases which implies that they could participate in the formation of amorphous phase at the grain boundaries. Mg^{2+} and Li^+ ions could also partially substitute Zn^{2+} in the crystal lattice of Zn_2SiO_4, leaving residual TiO_2.

3.3. Dielectric properties

Figs. 5a and b display the comparison of the dielectric permittivities and dissipation factors at room temperature of the studied willemite based ceramics in a frequency range of 100 Hz–2 MHz. The lowest dielectric permittivities of 6–6.4 were obtained for pure willemite and willemite doped with 5% AlF_3-CaB_4O_7. The introduction of a few percent of $MgTiO_3$ or Li_2TiO_3, as a second additive, besides 5% AlF_3-CaB_4O_7, allows for a further lowering of the sintering temperature of

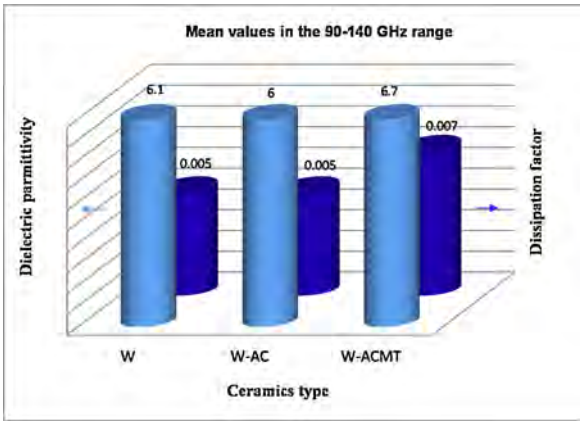

Fig. 8. Comparison of the mean values of the dielectric permittivity and dissipation factor at 20 °C in the 90–140 GHz range for Zn_2SiO_4 (W), Zn_2SiO_4 with 5% AlF_3-CaB_4O_7 (W-AC), and Zn_2SiO_4 with 5% AlF_3-CaB_4O_7 and 5% $MgTiO_3$ (W-ACMT).

willemite ceramic to a level that makes possible its cosintering with the cheap silver based pastes. However, a disadvantageous effect of a distinct increase in the dielectric permittivity was observed. It can be seen from Fig. 5a that the dielectric permittivities for the compositions containing as the additives 4% AlF_3-CaB_4O_7-Li_2TiO_3 and 5% AlF_3-CaB_4O_7 + 5% $MgTiO_3$ assume values in the range of 7.1–7.4.

Figs. 6a and b illustrate the frequency dependencies of the dielectric permittivity and dissipation factor in a range of 100 Hz–2 MHz for a few temperatures in the range from −30 to 150 °C for Zn_2SiO_4 ceramics with 5% AlF_3-CaB_4O_7 + 5% $MgTiO_3$, sintered at 930 °C. The dielectric permittivity varies from 7.1 to 7.5 in the studied ranges (Fig. 6a), increasing slightly with temperature. The dielectric permittivity and dissipation factor are lower and weakly dependent on frequency at lower temperatures. Above 10 kHz, as well as up to 80 °C, the dissipation factor does not exceed 0.004 in the whole frequency range (Fig. 6b). The higher values of dielectric permittivity and dielectric loss at lower frequencies and higher temperatures originate from the effect of space charge polarization.

The sintering temperature of the studied materials has a significant influence on both the dielectric permittivity and the dissipation factor. Fig. 7 illustrates the effect of the sintering conditions on the dielectric properties of willemite with 4% AlF_3-CaB_4O_7-Li_2TiO_3. It was found that both the increase in the sintering temperature and in the sintering time causes growing of the dielectric permittivity (Fig. 7a). This is due to the porosity reduction, which affects a dielectric permittivity enhancement. The dissipation factor is greater at the higher sintering temperature and the influence of sintering time is ambiguous (Fig. 7b).

These relationships are probably influenced by the contradictory factors. A higher sintering temperature and a longer sintering time promote the elimination of pores and consequently should reduce dielectric loss, although can also create the new sources of extrinsic losses associated with the precipitation of secondary crystalline phases, the appearance of amorphous phase and additional phase boundaries.

Table 1 and Fig. 8 show the mean values of the dielectric permittivity and dissipation factor of the investigated materials in the 90–140 GHz band. The dielectric permittivities are 6.1, 6 and 6.7 for Zn_2SiO_4, Zn_2SiO_4 with 5% AlF_3-CaB_4O_7 and Zn_2SiO_4 with 5% AlF_3-CaB_4O_7 + 5% $MgTiO_3$, respectively, while the dissipation factors of these materials do not exceed 0.005–0.007. The dielectric properties in the 90–140 GHz band of the examined willemite ceramics with and without the additives do not differ significantly.

Figs. 9a and b compare the dielectric permittivity and the dissipation factor as a function of frequency in the terahertz range for pure and doped willemite ceramics. The shape of both the dependencies for all tested compositions is very similar. For the developed materials based on doped Zn_2SiO_4, advantageous, low dielectric permittivities of 5.9–7 were attained in the frequency range of 0.15–1.5 THz. For each investigated material, the dielectric permittivity remains at a low, almost constant level in the 0.15–1.3 THz range, then increases reaching a small local maximum or inflection point at 2.2–2.5 THz and the maximum at frequency of 2.7–3 THz. The small local maximum or the inflexion point in the dielectric permittivity versus frequency plot that occurs at 2.2–2.5 THz is located at the similar frequency as the peak observed at 2.3 THz for pure willemite ceramics [19] and associated with a low frequency phonon mode. The dielectric permittivity values at 1 THz for willemite ceramics with the additives are: 6.1 for 5% AlF_3-CaB_4O_7, 6.8 for 4% AlF_3-CaB_4O_7-Li_2TiO_3 and 6.7 for 5% AlF_3-CaB_4O_7 + 5% $MgTiO_3$. In the THz range, the lowest dissipation factor values of 0.005-0.009 were observed at 0.5–1.2 THz. At the end of the usable measurement range (about 3 THz), for each studied material the distinct peaks of the dissipation factor were found at the similar frequencies as those for the dielectric permittivity.

The lowest dielectric permittivity similar to that of pure willemite, was obtained in the case of an addition of 5% AlF_3-CaB_4O_7. An increase in the dielectric permittivity of willemite ceramics after the introduction of the additives results from the fact that these materials (CaB_4O_7, Li_2TiO_3, $MgTiO_3$) have higher dielectric permittivities (11–22) than willemite, and to some extent from the improved densification due to the facilitated sintering process. The dissipation factor for the pure

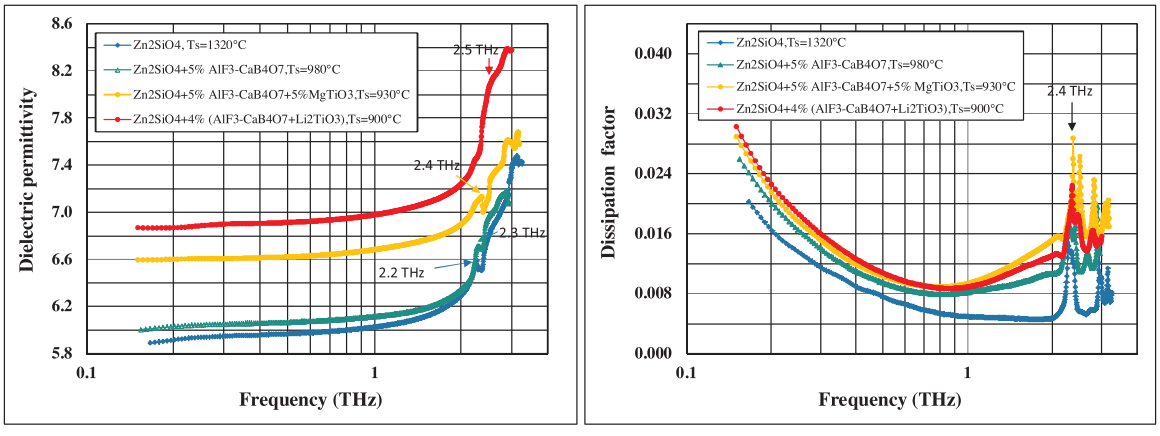

(a) (b)

Fig. 9. Comparison of the frequency dependencies of dielectric permittivity (a) and dissipation factor (b) at 20 °C in the 0.15–3 THz range for pure and doped Zn_2SiO_4 based ceramics.

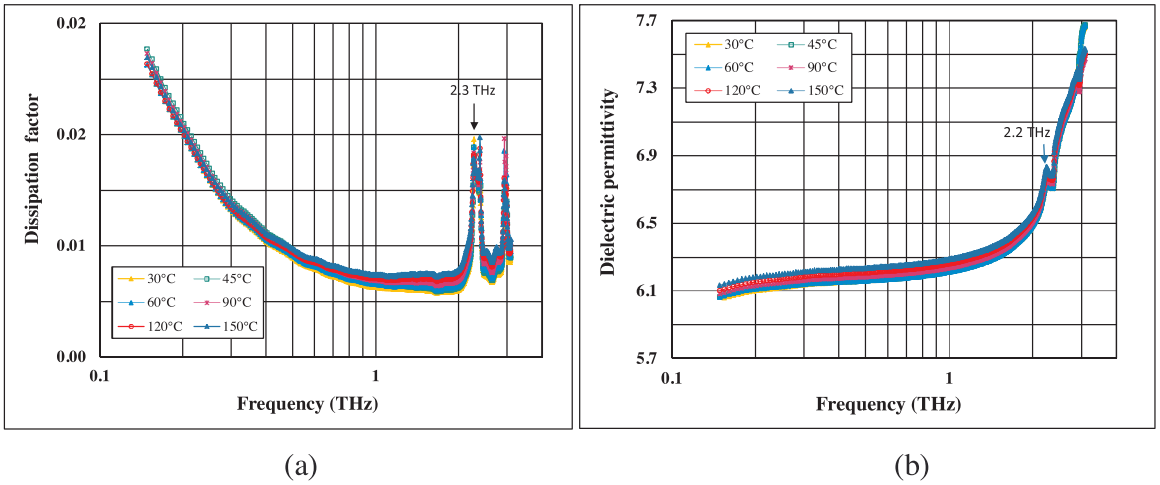

Fig. 10. Dielectric permittivity (a) and dissipation factor (b) in the temperature range 30–150 °C as a function of frequency in the range 0.15–3 THz for Zn_2SiO_4 ceramics sintered at 1320 °C.

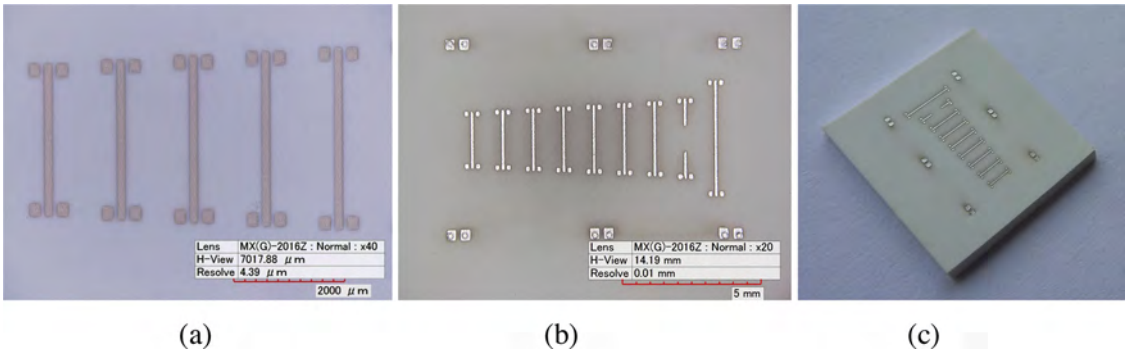

Fig. 11. (a), (b) Images from the optical microscope of the surface of the LTCC structure based on Zn_2SiO_4 doped with 4% AlF_3-CaB_4O_7-Li_2TiO_3, with a test pattern of Ag paths and *vias*: (a) a green sheet after screen printing, (b) substrate surface after firing, (c) general view of LTCC substrate.

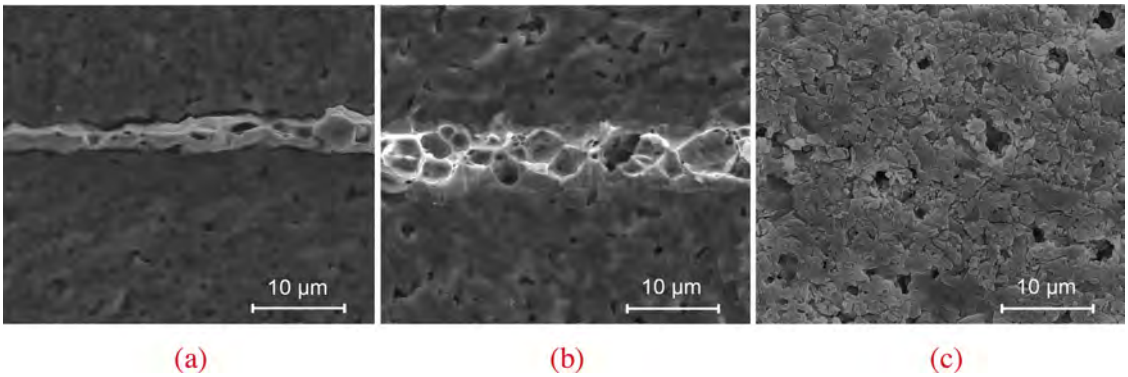

Fig. 12. SEM images of LTCC structures: (a) fractured cross-section of Zn_2SiO_4 with 5% AlF_3-CaB_4O_7, cosintered with AgPd layers at 980 °C, x 5000 (b) fractured cross-section of Zn_2SiO_4 with 4% AlF_3-CaB_4O_7-Li_2TiO_3, cosintered with Ag layers at 900 °C, x 5000, (c) chemically etched cross-section of the ceramic layer of Zn_2SiO_4 with 4% AlF_3-CaB_4O_7-Li_2TiO_3, sintered at 900 °C, x 5000.

willemite ceramics is distinctly lower than that for the doped ceramics. This is probably related to the scattering of phonons at the phase boundaries of the secondary crystalline phases or in the region of the glassy phase created with the participation of the introduced additives.

Similarly as in the lower frequency range, an increase in the sintering temperature or the sintering time affects a slight increase in the dielectric permittivity and the dissipation factor in the terahertz range.

In Figs. 10a and b the dielectric permittivity and the dissipation factor of pure Zn_2SiO_4 ceramics sintered at 1320 °C are depicted as a function of frequency in the range of 0.15–3 THz for a few temperatures from the range 30–150 °C. In general, both the dielectric permittivity and the dissipation factor increase slightly with growing temperature and the same shape of the plots is preserved for each temperature. For 1 THz, the dielectric permittivity increases from 6.24 at 30 °C to 6.28 at 150 °C. It was found that the position of the characteristic peak of both the real part and the imaginary part of permittivity, observed at 2.2–2.4 THz, does not depend on temperature in the 20–150 °C range. This implies that the phenomena related to this local maximum are not thermally activated processes. The weak temperature dependence of the dielectric permittivity is a very advantageous feature that ensures good temperature stability of a substrate made of willemite ceramics.

As can be seen from the comparison given in Table 1, the dielectric

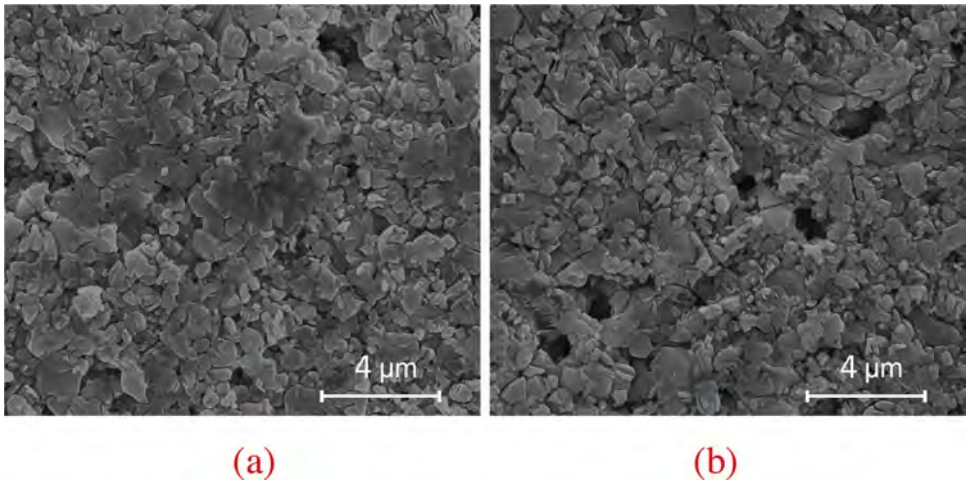

Fig. 13. SEM images of the chemically etched cross-sections of: (a) Zn_2SiO_4 ceramic with 5% AlF_3-CaB_4O_7, sintered at 980 °C, x 8000, (b) Zn_2SiO_4 ceramic with 5% AlF_3-CaB_4O_7 + 5% $MgTiO_3$, sintered at 930 °C, x 8000.

permittivity values of the analyzed willemite based materials at 1 THz are slightly lower than those at 1 MHz and very close to the mean values in the 90–140 GHz band. This effect stems from the fact that with increasing frequency the changes of several types of polarization (space charge, orientation, ionic) cannot keep pace with the quick changes of *ac* electric field, and at THz frequencies the real part of permittivity is determined mainly by electronic polarization. In general, the frequency dependence of the dielectric permittivity in three studied frequency ranges is weak which is advantageous for the microwave and submillimeter wave applications.

It follows from Table 1 that the dissipation factor at 1 MHz and its mean value in the 90–140 GHz band are lower than that at 1 THz. Otherwise that it is in the Hz-MHz range, the extrinsic losses associated with microstructure imperfections, grain boundaries, microcracks, etc., have a small impact in the THz range, where predominate the intrinsic losses determined by the crystal structure and related to the phonon interactions.

According to the model of the damped oscillator in the range of microwaves and submillimeter waves, corresponding to the frequencies much smaller than the phonon frequencies, one should expect that the real part of the permittivity ε' (the dielectric permittivity) is independent of frequency and its imaginary part ε'' (proportional to the dissipation factor $tg\delta = \varepsilon''/\varepsilon'$) increases with an increase in frequency [3]. In general, the frequency dependencies of the dielectric permittivity and dissipation factor observed in this work agree with the theoretical expectations.

3.4. LTCC structures

Fig. 11a shows the optical microscope image of the surface of a test pattern of the 150 μm wide Ag conductive paths, screen printed onto the green tape made of Zn_2SiO_4 with 4% AlF_3-CaB_4O_7-Li_2TiO_3. Owing to the high smoothness of the obtained green tape, a very good precision of the pattern, with the sharp and even path edges, was attained. Figs. 11b and c illustrate the LTCC structure based on this tape after firing at 900 °C for 1 h. The cooperation of the ceramic substrate with the conductive layers is very good and the structure is not distorted. After firing, the conductive paths retained a high edge sharpness, *vias* were properly filled and provided the good electrical contact between the conductive layers on the surface and within the structure. The shrinkage was significant, at a level of about 20%, which is typical for the LTCC elements.

Fig. 12a presents the microstructure of the fractured cross-section of a test LTCC substrate based on willemite ceramic with 5% AlF_3-CaB_4O_7. The analysis of the images from the optical and scanning microscopes revealed compatibility of this material with the AgPd and Pt commercial conductive pastes. The EDS analysis showed the uniform composition of the ceramic layers with no additional phases precipitated inside these layers or at the interphase of the ceramic layer and the conductive thick film. Fig. 12b shows the SEM image of the fractured cross-section of the multilayer structure based on Zn_2SiO_4 with 4% AlF_3-CaB_4O_7-Li_2TiO_3. The ceramic layers are homogeneous, well sintered, with a small closed porosity. The cooperation with the conductive silver layers is very good. Figs. 12c, 13a and b illustrate the SEM images of the polished and chemically etched cross-sections of Zn_2SiO_4 ceramics with 4% AlF_3-CaB_4O_7-Li_2TiO_3, 5% AlF_3-CaB_4O_7 and 5% AlF_3-CaB_4O_7 + 5% $MgTiO_3$, respectively. For all the investigated materials, a similar, dense and fine-grained microstructure was revealed with the grain sizes in a range of 0.5–3 μm.

4. Conclusions

Three applied additives, containing AlF_3, CaB_4O_7, Li_2TiO_3 and $MgTiO_3$, effectively lowered the sintering temperature of willemite ceramics to a level of 900–980 °C, suitable for cofiring with the commercial Ag and Ag-Pd conductive pastes. The XRD analysis indicated that the introduced additives did not precipitate as secondary phases but rather reacted with the main willemite phase or participated in the formation of the amorphous phase. For the developed materials based on the doped Zn_2SiO_4, low dielectric permittivities were attained in a broad investigated frequency range of 100 Hz–3 THz. The frequency and temperature dependencies of the dielectric permittivities of these materials were weak at frequencies exceeding 100 kHz. At 1 THz, the dielectric permittivities were low, assuming values of 6–6.8, whereas the dissipation factor values were relatively low, at a level of 0.005-0.009. A higher sintering temperature caused a slight increase in the dielectric permittivity. Owing to the low sintering temperature, compatibility with the commercial conductive thick film pastes and the desired dielectric properties at high frequencies, the developed ceramics are good candidates for LTCC substrates destined for the microwave and submillimeter wave applications.

Declaration of Competing Interest

The authors declare that they have no known competing financial interests or personal relationships that could have appeared to influence the work reported in this paper.

Acknowledgment

The work was financed by the National Center for Research and Development, Poland, under grants No. PBS3/A3/18/2015 and No. PBS3/B3/30/2015.

References

[1] K. Maex, M.R. Baklanov, D. Shamiryan, F. Iacopi, S.H. Brongersma, Z.S. Yanovitskaya, Low dielectric constant materials for microelectronics, J. Appl. Phys. 93 (2003) 8793–8841, https://doi.org/10.1063/1.1567460.

[2] M.T. Sebastian, R. Ubic, H. Jantunen, Low-loss dielectric ceramic materials and their properties, Int. Mater. Rev. 60 (2015) 392–412, https://doi.org/10.1179/1743280415Y.0000000007.

[3] J. Petzelt, S. Kamba, Submillimetre and infrared response of microwave materials: extrapolation to microwave properties, Mater. Chem. Phys. 79 (2003) 175–180, https://doi.org/10.1016/S0254-0584(02)00269-9.

[4] C. Hu, P. Liu, Microwave dielectric properties of SiO_2 ceramics with addition of Li_2TiO_3, Mater. Res. Bull. 65 (2015) 132–136, https://doi.org/10.1016/j.materresbull.2015.01.034.

[5] L. Li, C.H. Liu, J.Y. Zhu, X.M. Chen, B_2O_3-modified fused silica microwave dielectric materials with ultra-low dielectric constant, J. Eur. Ceram. Soc. 35 (2015) 1799–1805, https://doi.org/10.1016/j.jeurceramsoc.2014.12.016.

[6] D. Szwagierczak, B. Synkiewicz, J. Kulawik, Low dielectric constant composites based on B_2O_3 and SiO_2 rich glasses, cordierite and mullite, Ceram. Int. 44 (2018) 14495–14501, https://doi.org/10.1016/j.ceramint.2018.05.064.

[7] T. Sugiyama, T. Tsunooka, K.I. Kakimoto, H. Ohsato, Microwave dielectric properties of forsterite-based solid solutions, J. Eur. Ceram. Soc. 26 (2006) 2097–2100, https://doi.org/10.1016/j.jeurceramsoc.2005.09.102.

[8] B.K. Choi, S.W. Jang, E.S. Kim, Dependence of microwave dielectric properties on crystallization behaviour of $CaMgSi_2O_6$ glass-ceramics, Mater. Res. Bull. 67 (2015) 234–238, https://doi.org/10.1016/j.materresbull.2014.11.031.

[9] B.C. Babu, S. Buddhudu, Dielectric properties of willemite Zn_2SiO_4 nano powders by sol-gel method, Phys. Proc. 49 (2013) 128–136, https://doi.org/10.1016/j.phpro.2013.10.019.

[10] E. Ozel, H. Yurdakul, S. Turan, M. Ardit, G. Cruciani, M. Dondi, Co-doped willemite ceramic pigments: technological behaviour, crystal structure and optical properties, J. Eur. Ceram. Soc. 30 (2010) 3319–3329, https://doi.org/10.1016/j.jeurceramsoc.2010.08.013.

[11] M.A. Eidem, B.R. Orton, A. Whitaker, Phase equilibria in the system ZnO-B_2O_3-SiO_2 at 950°C, J. Mater. Sci. 22 (1987) 4139–4143, https://doi.org/10.1007/BF01133370.

[12] Y. Guo, H. Ohsato, K.I. Kakimoto, Characterization and dielectric behavior of willemite and TiO_2-doped willemite ceramics at millimeter-wave frequency, J. Eur. Ceram. Soc. 26 (2006) 1827–1830, https://doi.org/10.1016/j.jeurceramsoc.2005.09.008.

[13] V. Chaware, R. Deshmukh, C. Sarode, S. Gokhale, G. Phatak, Low-temperature sintering and microwave dielectric properties of Zn_2SiO_4 ceramic added with crystalline zinc borate, J. Electron. Mater. 44 (7) (2015) 2312–2320, https://doi.org/10.1007/s11664-015-3762-0.

[14] J.S. Kim, N.H. Nguyen, J.B. Lim, D.S. Paik, S. Nahm, J.H. Paik, J.H. Kim, Low-temperature sintering and microwave dielectric properties of the Zn_2SiO_4 ceramics, J. Am. Ceram. Soc. 91 (2008) 671–674, https://doi.org/10.1111/j.1551-2916.2007.02187.x.

[15] G. Dou, D. Zhou, M. Guo, S. Gong, Low-temperature sintered Zn_2SiO_4–$CaTiO_3$ ceramics with near-zero temperature coefficient of resonant frequency, J. Alloys. Compd. 513 (2012) 466–473, https://doi.org/10.1016/j.jallcom.2011.10.089.

[16] G. Dou, M. Guo, Y. Li, J. Lin, Effects of low melting point materials on sinterability and microwave dielectric properties of X_2SiO_4–$CaTiO_3$ (X = Mg, Zn) for LTCC, J. Mater. Sci: Mater. Electron. 26 (2015) 9195–9199, https://doi.org/10.1007/s10854-015-3611-1.

[17] N.H. Nguyen, J.B. Lim, S. Nahm, J.H. Paik, J.H. Kim, Effect of Zn/Si ratio on the microstructural and microwave dielectric properties of Zn_2SiO_4 ceramics, J. Am. Ceram. Soc. 90 (2007) 3127–3130, https://doi.org/10.1111/j.1551-2916.2007.01891.x.

[18] S.R. Lukić, D.M. Petrović, M.D. Dramićanin, M. Mitrić, L. Dačanin, Optical and structural properties of Zn_2SiO_4:Mn^{2+} green phosphor nanoparticles obtained by a polymer-assisted sol-gel method, Scr. Mater. 58 (2008) 655–658, https://doi.org/10.1016/j.scriptamat.2007.11.045.

[19] L. Nedelcu, C.D. Geambasu, M.G. Banciu, A. Iwamae, T. Furuya, M. Tani, Submillimeter-wave properties of Zn_2SiO_4 ceramics, 40th International Conference on Infrared, Millimeter, and Terahertz Waves (IRMMW-THz), Hong Kong, China, 23–28 Aug, 2015, https://doi.org/10.1109/IRMMW-THz.2015.7327946.

[20] S. Kim, S.O. Yoo, Y.H. Kim, S.M. Jeong, H. Park, Microstructure, phase evolution and microwave dielectric properties of Li_2O and Ga_2O_3 doped zinc orthosilicate, Ceram.-Silikaty 61 (2017) 209–213, https://doi.org/10.13168/cs.2017.0018.

[21] Ferro, Low Temperature Co-Fired Ceramic Systems A6M-E High Frequency LTCC Tape System, October, Technical Data Sheet, 2018, https://www.ferro.com.

[22] A. Sasidharanpillai, C.H. Kim, C.H. Lee, M.T. Sebastian, H.T. Kim, Environmental friendly approach for the development of ultra-low firing Li_2WO_4 ceramic tapes, ACS Sustainable Chem. Eng. 6 (5) (2018) 6849–6855, https://doi.org/10.1021/acssuschemeng.8b00656.

[23] H. Yu, J. Liu, W. Zhang, S. Zhang, Ultra-low sintering temperature ceramics for LTCC applications: a review, J. Mater. Sci.: Mater. Electron. 26 (2015) 9414–9423, https://doi.org/10.1007/s10854-015-3282-y.

[24] N. Joseph, J. Varghese, M. Teirikangas, M.T. Sebastian, H. Jantunen, Ultra-low sintering temperature ceramic composites of $CuMoO_4$ through Ag_2O addition for microwave applications, Compos. Part B Eng. 141 (2018) 214–220, https://doi.org/10.1016/j.compositesb.2017.12.055.

[25] D. Zhou, L.X. Pang, D.W. Wang, I.M. Reaney, Novel water-assisting low firing MoO_3 microwave dielectric ceramics, J. Eur. Ceram. Soc. 39 (2019) 2374–2378, https://doi.org/10.1016/j.jeurceramsoc.2019.01.052.

[26] D. Zhou, L.X. Pang, D.W. Wang, Z.M. Qi, I.M. Reaney, High quality factor, ultralow sintering temperature $Li6B_4O_9$ microwave dielectric ceramics with ultralow density for antenna substrates, ACS Sustain. Chem. Eng. 6 (8) (2018) 11138–11143, https://doi.org/10.1021/acssuschemeng.8b02755.

[27] P.R. Bajurko, Millimeter wave permittivity and loss tangent measurements of LTCC materials, 21st International Conference on Microwave, Radar and Wireless Communications, MIKON 2016, Krakow, Poland, 9–11 May 2016, 2016, https://doi.org/10.1109/MIKON.2016.7492104.

[28] J.L. Ma, Z.F. Fu, P. Liu, B. Wang, Y. Li, Microwave dielectric properties of low-fired Li_2TiO_3-MgO ceramics for LTCC applications, Mater. Sci. Eng. B 204 (2016) 15–19, https://doi.org/10.1016/j.mseb.2015.10.007.

[29] C.L. Huang, C.L. Pan, S.J. Shium, Liquid phase sintering of $MgTiO_3$-$CaTiO_3$ microwave dielectric ceramics, Mater. Chem. Phys. 78 (2002) 11–115, https://doi.org/10.1016/S0254-0584(02)00311-5.

[30] C.L. Huang, C.L. Pan, W.C. Lee, Microwave dielectric properties of glass-forming oxides Zn-B-Si and dielectric ceramics $MgTiO_3$-$CaTiO_3$ for LTCC applications, J. Alloys. Compd. 462 (2008) L5–L8, https://doi.org/10.1016/j.jallcom.2007.07.114.

[31] H.K. Shin, H. Shin, S.Y. Cho, K.S. Hong, Phase evolution and dielectric properties of $MgTiO_3$-$CaTiO_3$-based ceramic sintered with lithium borosilicate glass for application to low temperature co-fired ceramics, J. Am. Ceram. Soc. 88 (2005) 2461–2465, https://doi.org/10.1111/j.1551-2916.2005.00453.x.

[32] F. Xu, M. Dong, W. Gou, J. Li, A. Qin, J. Wang, W. Fan, Rapid tuning of ZSM-5 crystal size by using polyethylene glycol or colloidal silicalite-1 seed, Microporous Mesoporous Mater. 163 (2012) 192–200, https://doi.org/10.1016/j.micromeso.2012.07.030.

[33] K.S. Jaw, C.K. Hsu, J.S. Lee, The thermal decomposition behaviors of stearic acid, paraffin wax and polyvinyl butyral, Thermochim. Acta 367-368 (2001) 165–168, https://doi.org/10.1016/S0040-6031(00)00680-8.

[34] L.A. Salam, R.D. Matthews, H. Robertson, Pyrolysis of polyvinyl butyral (PVB) binder in thermoelectric green tapes, J. Eur. Ceram. Soc. 20 (2000) 1375–1383, https://doi.org/10.1016/S0955-2219(99)00236-8.